



Capacity of axially loaded bored cast-in-place piles socketed in Dubai limestone

Amr F. Elhakim¹

Received: 5 March 2022 / Accepted: 26 May 2022 / Published online: 20 June 2022
© Springer Nature Switzerland AG 2022

Abstract

Piles are used as the foundation of choice in various engineering projects including multi-story buildings, bridges and offshore structures. This paper analyzes the axial capacity of bored cast-in-place rock socketed piles from eight full-scale load tests in Dubai. Two of the tested piles are instrumented providing data about the load transfer along the pile shaft and load carried by tip resistance. An extensive subsurface investigations program is performed at the project site to properly characterize the properties of the different ground layers. Using the pile load tests results, the ultimate pile capacities are computed using both Chin and Decourt methods. The analysis of the instrumented load tests shows that no load is transferred to the pile tip. Thus, only side shaft resistance is mobilized during loading. The shaft side resistance is computed for all the load tests using the load–displacement measurements. The back-calculated capacities are compared with values obtained using a plethora of empirical correlations to identify the most suitable for use in Dubai limestone. The empirically computed shaft capacities exhibit a large degree of variability. A site-specific correlation is deduced using the available data.

Keywords Rock socket · Bored pile · Dubai limestone · Pile capacity

Introduction

Piles are used to support many mid-rise and high-rise buildings in Dubai, United Arab Emirates. The reasons for using piles include high structural loads and the presence of unsuitable surface soils (e.g., low bearing capacity, highly compressible, susceptible to liquefaction). The use of socketed piles is appropriate for sites with shallow loose sand underlain by rock. In such conditions, substantial side shaft resistance is developed even at small pile displacements [1, 2]. Loads are transferred to the bearing rock layer through two mechanisms: side and tip resistances. The load distribution between both mechanisms depends on the relative stiffness of the pile and rock in addition to the properties of the pile–rock interface [3]. There are several correlations to determine the pile resistance in rock [e.g., 4–12]. These correlations are empirically based exhibiting large variability in predicting pile capacities. The variability is attributed to the different factors affecting the capacity which include the method of construction, regional rock mass properties and

pile–rock interface properties. Some correlations are developed for certain geological formations using specific construction techniques which may be inapplicable to other regions [13]. Thus, it is important to conduct full-scale load tests to confirm the pile capacity. In this paper, the load–displacement response curves of eight full-scale load tests performed in Dubai are analyzed to define the most suitable method to compute the pile capacity socketed in Dubai limestone. Two of these piles are instrumented to determine the load transfer along the pile shaft and load carried by the pile tip.

Subsurface ground conditions

A proper pile design requires reliable characterization of the subsurface ground conditions. An extensive subsurface site investigations program comprised of 33 boreholes drilled to depths varying between 25-m and 50-m is performed at the project location. In the sand layers, Standard Penetration tests are conducted at various depths in all boreholes to assess the in situ sand relative density. Disturbed soil samples are obtained from different depths to perform index tests which include grain size distribution and specific gravity. Core specimens are extracted from the rock layers for laboratory tests

✉ Amr F. Elhakim
aelhakim@eng.cu.edu.eg

¹ Department of Public Works, Faculty of Engineering, Cairo University, Giza, Egypt

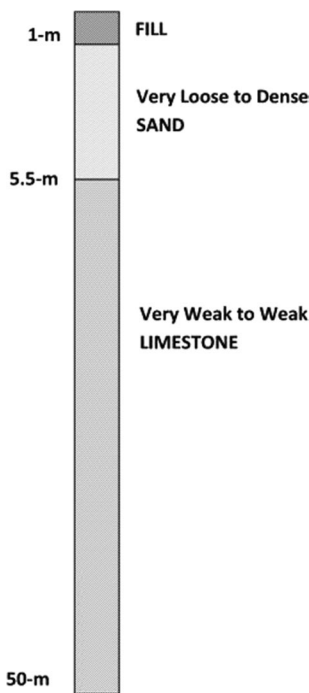


Fig. 1 Representative Borehole Log

to define its strength and deformation properties. The Core Recovery (CR) and Rock Quality Designation (RQD) are calculated from field logs to identify the rock mass properties.

A representative borehole log at the project site is shown in Fig. 1. The subsurface ground profile is comprised of a top layer of fill with thicknesses varying between 0.3-m and 1.5-m with an average depth of 1-m. The fill layer is quite heterogeneous described as grayish brown silty fine to medium sand with gravel and pieces of asphalt. No SPT-N values were recorded within this layer. This stratum is underlain by a cohesionless calcareous sand layer with thicknesses ranging between 3.1-m up to 6.45-m, which can be divided into 2 layers. An upper one characterized with SPT-N values which typically vary between 0 and 20 but not exceeding 30. The thickness of this layer varies between 4-m and 5-m. The SPT-N values increase in the lower sand layer reaching 50 close to the soil–rock interface. A SPT-N value of zero indicates that the weight of the rods and hammer results in the sampler to drop through the whole test section (30-cm) which is characteristic of very loose sand. The measured SPT-N values are presented in Fig. 2-a. Similar subsurface ground conditions are encountered in other locations in Dubai [e.g., 14, 15]. The large variability of the degree of compactness of the sand layer is typical of these marine deposits in

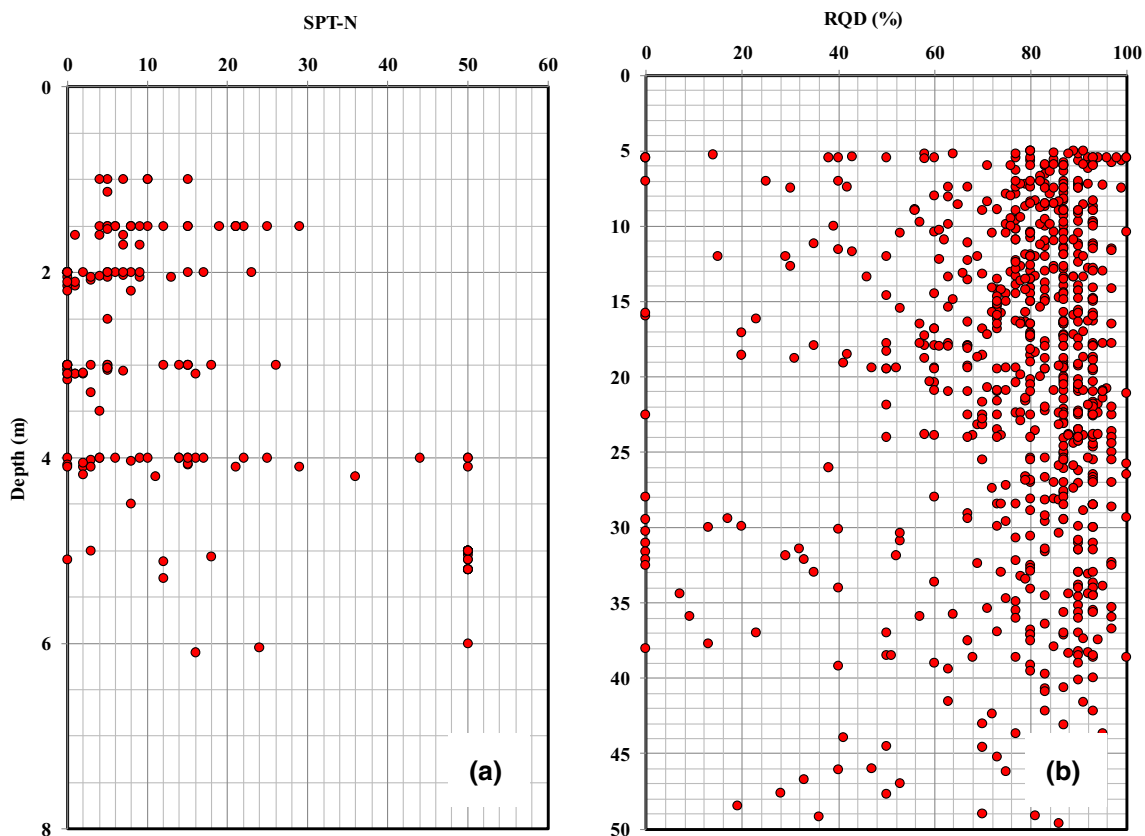


Fig. 2 a Measured SPT-N values versus depth b RQD versus depth

Dubai as reported by Poulos [16]. Very weak to weak limestone is encountered under the cohesionless sand layer. A total of 728 RQD measurements are computed within the rock stratum as shown in Fig. 2-b. Approximately 92% of the RQD are higher than 50%, and thus, the rock mass is classified as fair to excellent with an average RQD of 77% [17]. Unconfined compressive strength tests are performed on the extracted rock specimens as presented in Figs. 3-a. The values of the unconfined compressive strength vary between 0.54 MPa and 11.64 MPa with an average of 3.37-MPa. Thus, the tested rock specimens are classified as very weak to weak according to the National Engineering Handbook [18]. Poulos and Davids [14] report similar properties for both intact and rock mass properties in Dubai. Figure 3-b shows the calcium carbonate contents for the sand and rock samples which range between 17 and 65% with a mean value of 49.2%. According to ARGEMA [19], rocks with carbonate contents higher than 30% are described as carbonate.

Pile load tests

Full-scale load tests are conducted on bored piles in accordance with the maintained load test method of ASTM D1143 / D1143 M-20 [20]. The load tests are performed on six 1.2-m diameter piles and two 1-m diameter piles. The lengths of the piles range between 17-m and 25-m below ground surface with rock socket lengths that vary between 11.5-m and 19.8-m. Table 1 summarizes the basic data for the tested piles. The pile head movement is monitored at four points by 4 displacement dial gauges which are mounted on independent reference beams. The dial gauges have a range of 0 to 50-mm with an accuracy of 0.025-mm. Figure 4 shows the load–displacement response of all the tested piles. The maximum applied loads range between 10.52-MN and 30.76-MN.

The pile ultimate capacity is reached with the onset of failure associated with the stress reaching a constant value

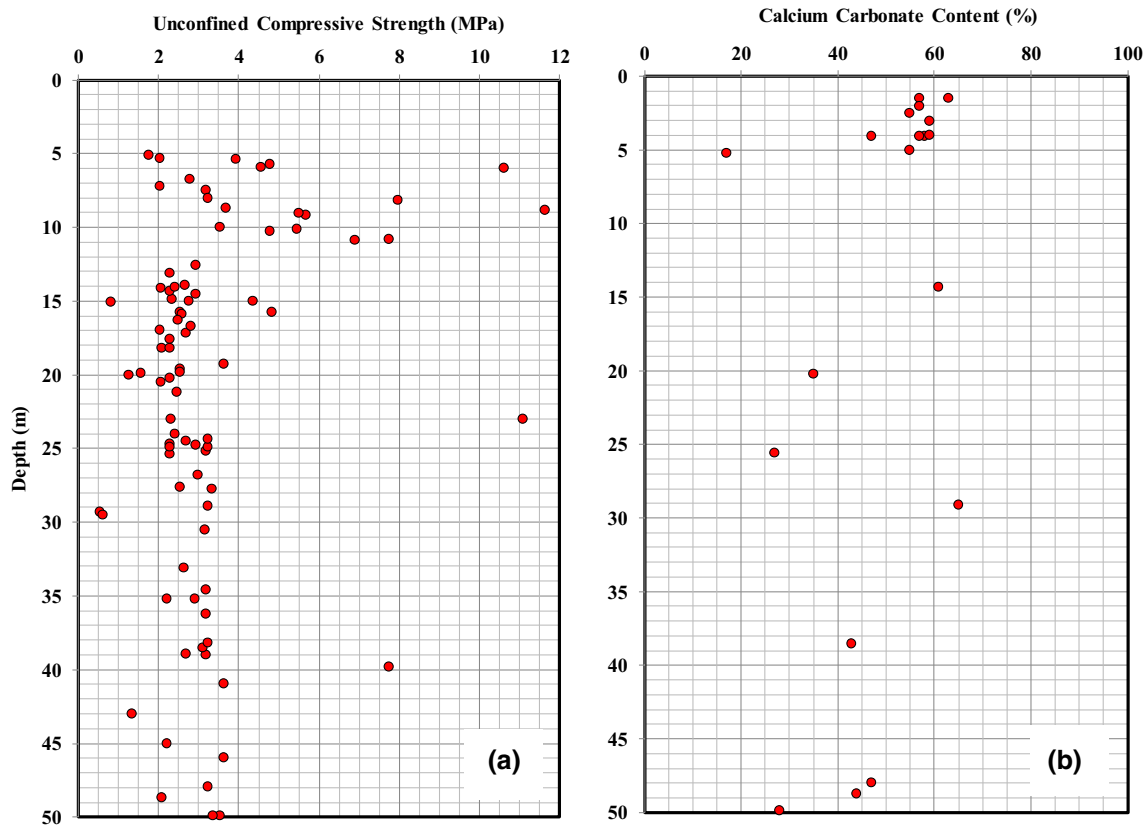
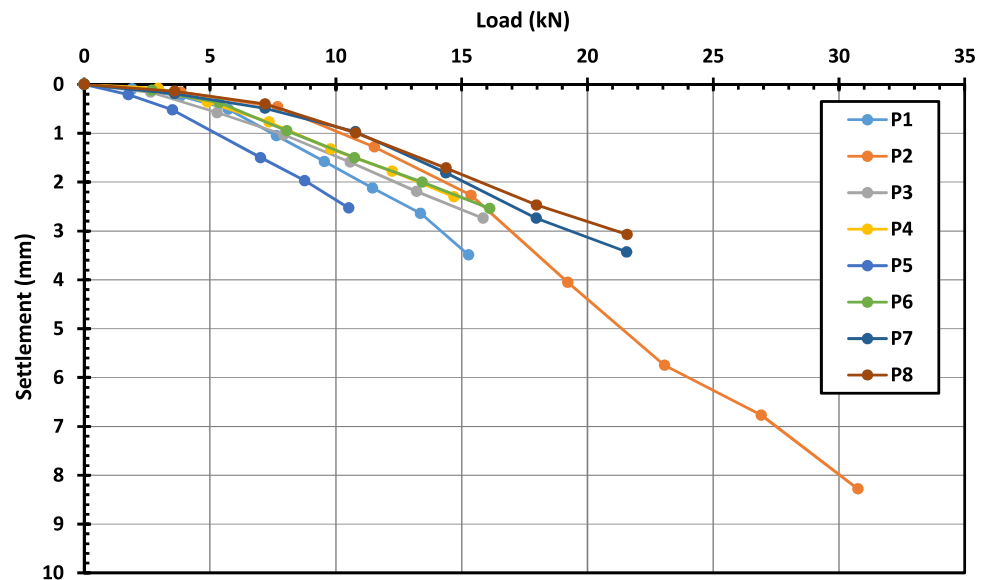


Fig. 3 a Unconfined Compressive Strength versus depth b Calcium Carbonate Content versus depth

Table 1 Basic data for tested piles

Pile number	Diameter d (m)	Total length L_t (m)	Socket length L_s (m)	Maximum load (MN)	Maximum settlement (mm)
P1	1.0	17	11.5	15.28	3.49
P2	1.2	25	19.8	30.76	8.28
P3	1.2	18.95	15.12	15.86	2.74
P4	1.2	18.68	14.12	14.70	2.30
P5	1.0	16.68	12.12	10.52	2.53
P6	1.2	21.08	18.12	16.12	2.54
P7	1.2	21.83	19.12	21.57	3.43
P8	1.2	22.88	19.12	21.58	3.07

Fig. 4 Full-scale load–displacement response of tested piles

or peaking. Examining the load test data, none of the test piles reach failure. Several techniques have been developed to provide a consistent framework to evaluate the failure load [21–26]. Akguner and Kirkit [2] found that mathematically based graphical methods [e.g., 23, 26] are suitable for interpreting load tests of socketed piles because of small pile displacements. Elhakim [27] demonstrates that the methods proposed by Brinch Hansen [21]; De Beer [22] and Amar et al. [25] are not suited for load tests with limited displacements, while the methods suggested by Chin [23] and Decourt [26] are more suited for such cases. Accordingly,

the ultimate loads for all the load tests are evaluated using both Chin and Decourt methods.

The simple hyperbola is one of the simplest formulae to represent the non-linear load–displacement response and only requires two constants. Accordingly, it has been used to evaluate the capacity of piles. Chin [23] plots the pile head displacement on the X-axis versus the pile displacement divided by the applied load on the Y-axis. Using these transformed axes, the data are represented by a straight line with the ultimate pile capacity as the reciprocal of the slope of this line, as presented in Fig. 5. Decourt [26] proposes

Fig. 5 Schematic Diagram of Chin Transformed Axes to Determine the Pile Axial Capacity

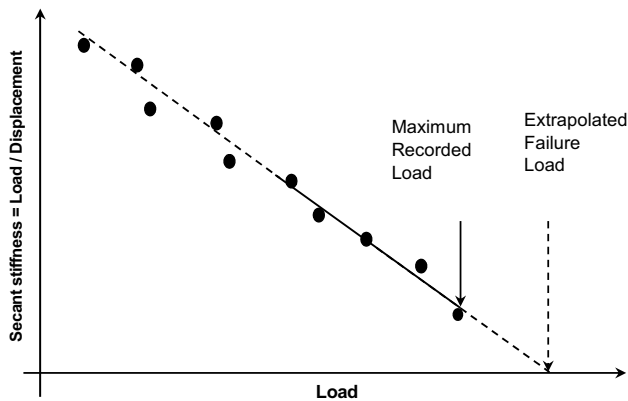
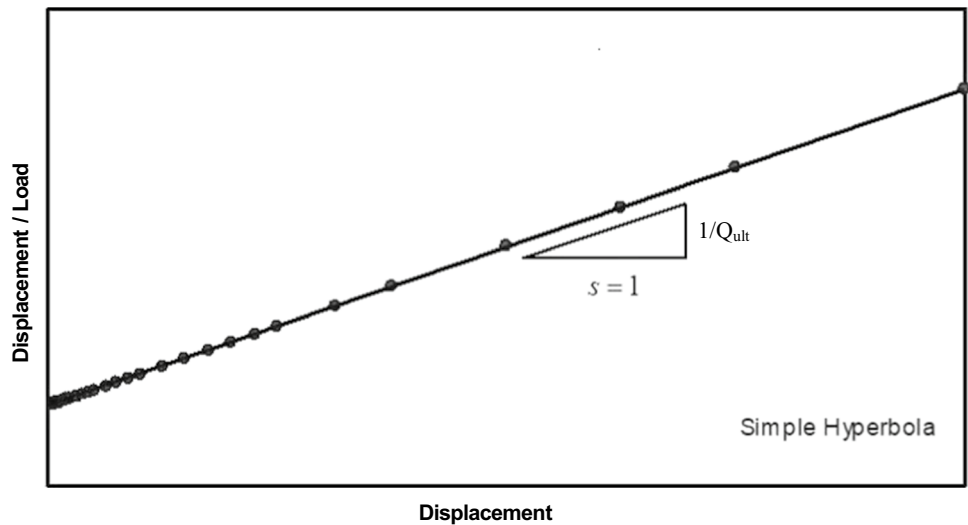


Fig. 6 Schematic Diagram of Decourt’s Method to Determine the Pile Axial Capacity

plotting the secant modulus ($K_s = Q/s$) versus the applied load (Q) to evaluate the ultimate pile capacity (Q_{ult}) which is equivalent to zero secant modulus ($K_s = 0$). Similar to Chin’s technique, a straight line is fitted to the data and the ultimate pile capacity is determined by extrapolating the data to reach a zero-secant modulus (intercept with the X-axis), as illustrated in Fig. 6. Table 2 summarizes the maximum applied load compared with both Chin and Decourt ultimate loads. It is clear that the applied loads are quite smaller than either Chin or Decourt ultimate capacities. This confirms that none of the piles was loaded to its ultimate capacity. For comparison, the maximum applied loads are plotted versus the interpreted ultimate capacities obtained from both Chin and Decourt methods as shown in Fig. 7a and b, respectively. As presented, Chin’s ultimate capacity is 69% higher than the maximum applied load. Similarly, Decourt’s ultimate capacity is 80% higher than the maximum applied load. Figure 7c shows the relation between Chin and Decourt ultimate loads indicating that the ultimate capacity using Decourt’s technique is on average 6% higher than Chin’s method.

Table 2 Summary of maximum applied loads and interpreted ultimate capacities

Pile number	Maximum load (MN)	Chin ultimate load (MN)	Decourt ultimate load (MN)
P1	15.28	25.0	27.3
P2	30.76	45.9	49.0
P3	15.86	33.3	33.0
P4	14.70	33.3	29.5
P5	10.52	25.0	29.0
P6	16.12	28.57	32.0
P7	21.57	33.3	34.2
P8	21.58	33.3	39.9

Instrumented pile load test results

Piles P1 and P2 are instrumented to examine the load transfer along pile shaft. Four strain gauges are welded to the pile reinforcing steel. Vibrating wire strain gauges are made of two end blocks connected with a tensioned steel wire. As the medium which includes the strain gauge is strained, relative movement develops between the end blocks. The gauges are connected to a readout unit which records the pile

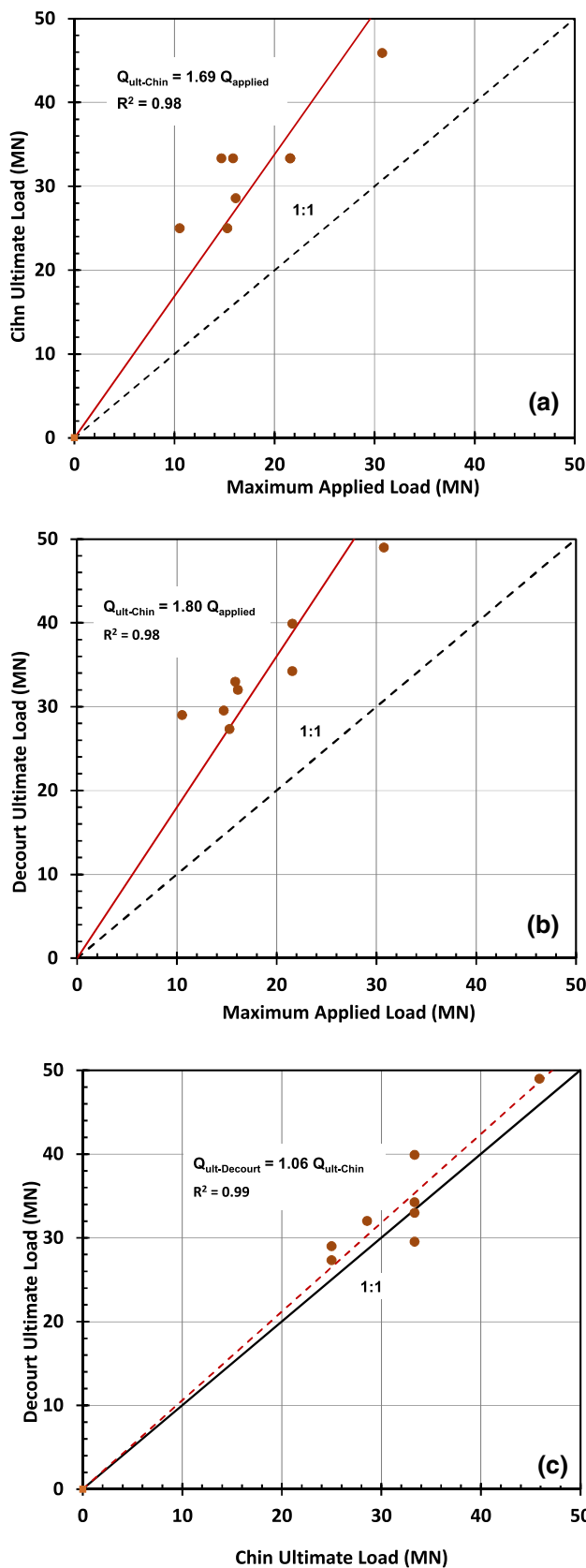


Fig. 7 a Maximum Applied load versus Chin ultimate load; b Maximum Applied load versus Decourt ultimate load; c Chin versus Decourt Ultimate Loads

shaft deformations. This results in a change in the resonant frequency of the wire. For pile P1, the strain gauges are placed 1-m, 5.5-m (approximate soil/rock interface), 10-m and 16-m (1-m above pile toe level) below the pile cut-off level. Similarly, for pile P2, the strain gauges are placed 1-m, 5.2-m (approximate soil/rock interface), 10.5-m, 17.5-m and 24-m (1-m above pile toe level) below the pile cut-off level.

The pile load–unload displacement results for piles P1 and P2 are presented in Fig. 8. The highest applied loads are 15.28-MN and 30.76-MN for piles P1 and P2, respectively. For pile P1, the highest and residual recorded pile head movements are 3.49-mm and 0.36-mm, respectively. Similarly, for pile P2, the maximum and residual pile head movements are 8.28-mm and 1.36-mm, respectively. Figure 9a and b shows the load transfer and the percentage of the applied load versus depth for pile P1. The percentage of the applied load transferred to a depth of 16-m (1 m above the pile tip) varies between 0% and 8.6% corresponding to 25% and 100% of the maximum applied load. Similarly, Fig. 10a and b shows the load transfer curves and percentage of applied load versus depth for pile P2, respectively. The load transferred to a depth of 24-m (1-m above pile tip) ranges between 0 and 11.5% for 25% and 100% of the maximum applied load, respectively. Table 3 summarizes the main results from the pile load tests on piles P1 and P2.

The variation of the pile shaft resistance with depth is presented in Figs. 11-a and 11-b for 25%, 50%, 62.5%, 75%, 87.5% and 100% of the maximum applied loads, respectively. The average side resistance is computed based on the strain gauge measurements. The shaft resistance in the top sand layer increases with depth down to the rock stratum. Table 4 summarizes the average side resistance versus depth for piles P1 and P2.

Figure 12a shows the mobilized side resistance versus pseudo-strain (pile head movement to pile diameter) at depths of 5.5-m, 10-m and 16-m for pile P1. For the shaft in the sand layer, the resistance increases with the increase in pile head movement reaching a peak strength of 166.8-kPa at a pseudo-strain of 0.11%. Loading the pile beyond the peak load, strain softening is observed with the shaft side resistance reaching 148.1-kPa corresponding to a pseudo-strain of 0.35%. On the other hand, the shaft side resistance in the rock layer does not reach a peak value up to the maximum recorded strain of 0.35%. Similarly, the mobilized side resistance for pile P2 is plotted versus pseudo-strain in Fig. 12b at depths of 5.2-m, 10.5-m, 17.5-m and 24-m. For the shaft resistance in the sand layer, the ultimate shaft side resistance of 249-kPa is achieved at a pseudo-strain of 0.34% with a reduction in resistance with further loading. The recorded shaft resistances in the rock layer do not reach failure up the maximum pseudo-strain of 0.69%. Based on

Fig. 8 Load-unload displacement response curves for piles P1 and P2

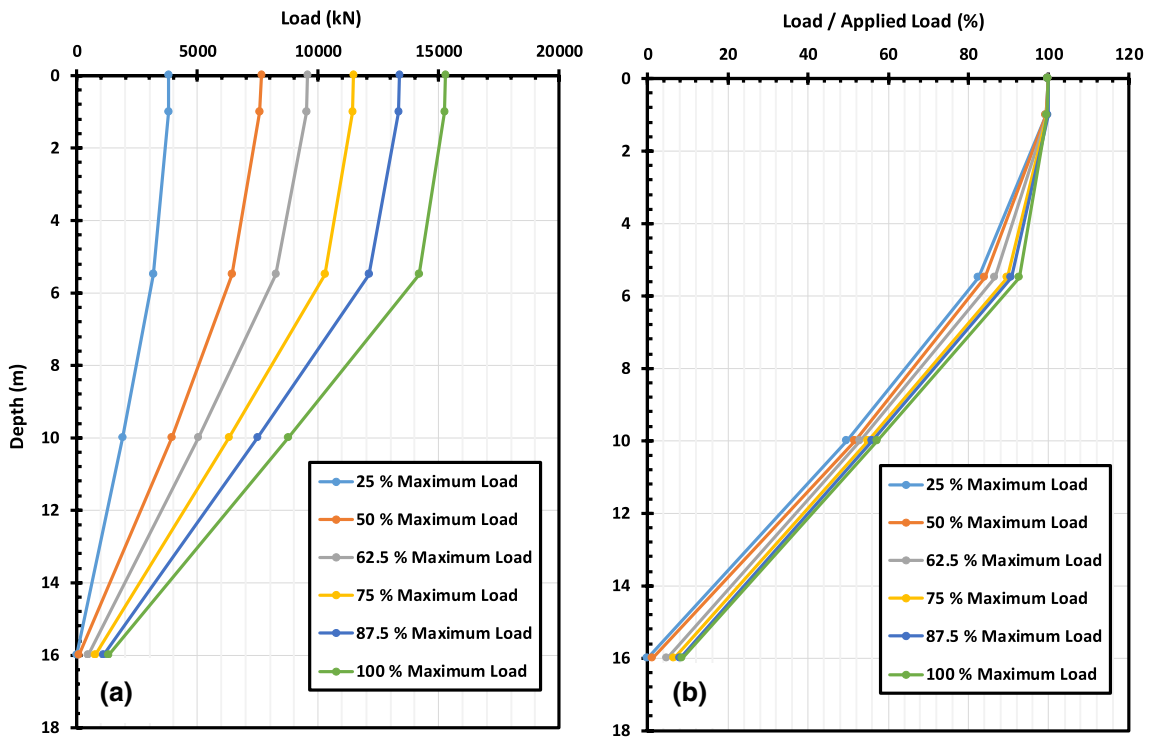
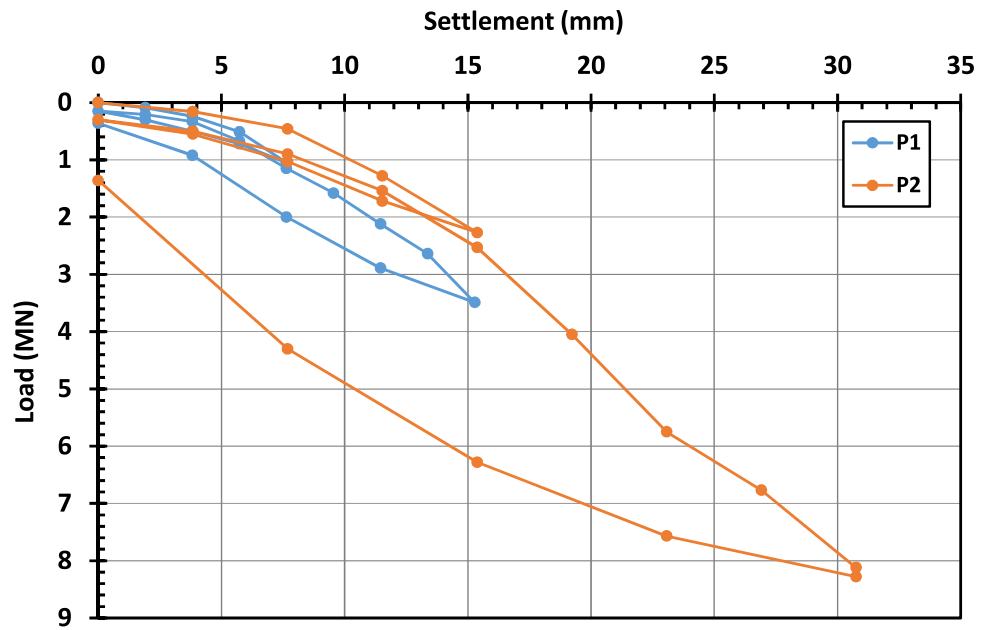


Fig. 9 a Load transfer versus depth; b Percentage of applied load transfer versus depth for pile P1

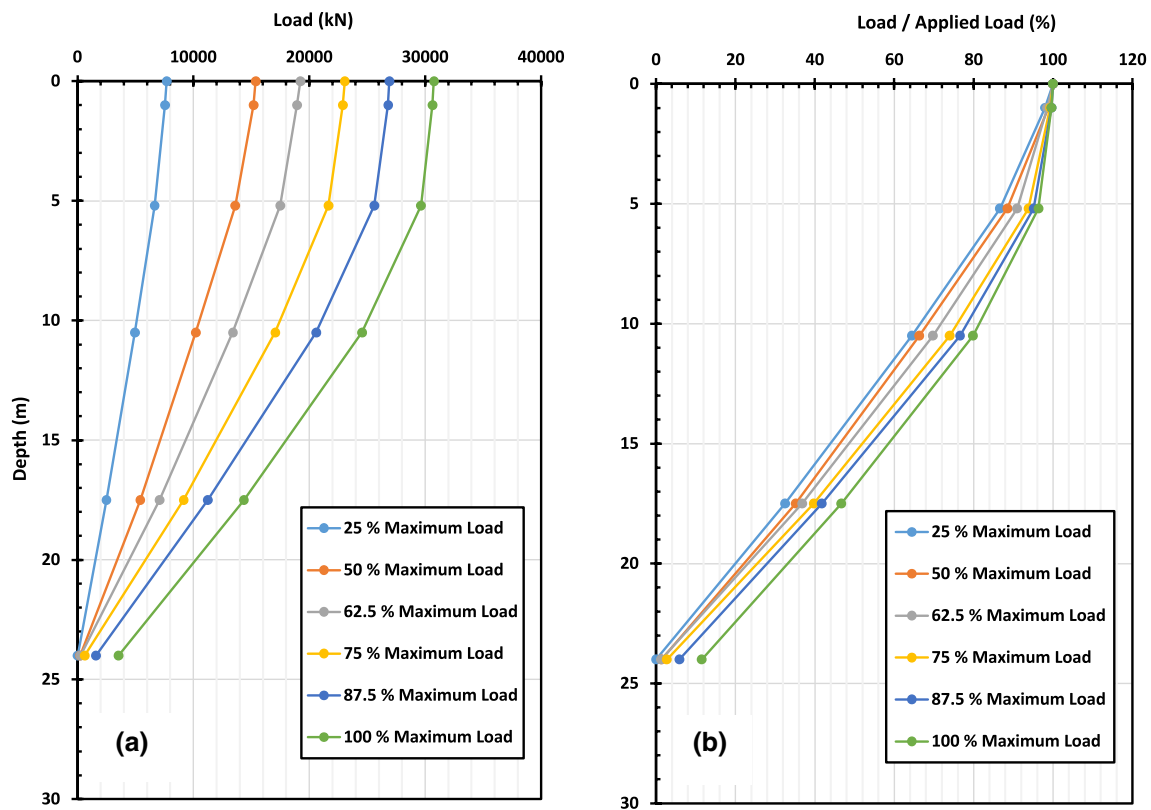


Fig. 10 a Load transfer versus depth b Percentage of applied load transfer versus depth for pile P2

Table 3 Summary of load test results for piles P1 and P2

	P1	P2
Maximum applied load (MN)	15.28	30.76
Maximum head movement (mm)	3.49	8.28
Residual head movement (mm)	0.36	1.36
% Load at 1-m above Pile Tip (25% of the maximum applied load)	0	0
% Load at 1-m above Pile Tip (100% of the maximum applied load)	8.6	11.5

the rock side resistance, no load is transferred to the pile tip with all the load being carried by shaft resistance. As illustrated from the measured data, the shaft resistance in the rock layer is much higher compared to sand with the ratio of the rock to sand shaft resistances of 4.9 and 10.7 at 50% and

100% of the maximum applied load for pile P1, respectively. Similarly, the ratios of the rock to sand side resistances are 3.7 and 10.7 for pile P2. Thus, the contribution of the sand layer to pile capacity is insignificant, especially for higher loads. Accordingly, the sand shaft resistance is ignored in the analysis of the capacities of the pile rock sockets.

Rock socket side resistance

The ultimate side resistance of the rock socket is computed as the summation of the shear resistance over the socket surface. For a circular pile, the pile socket capacity is calculated according to the below equation.

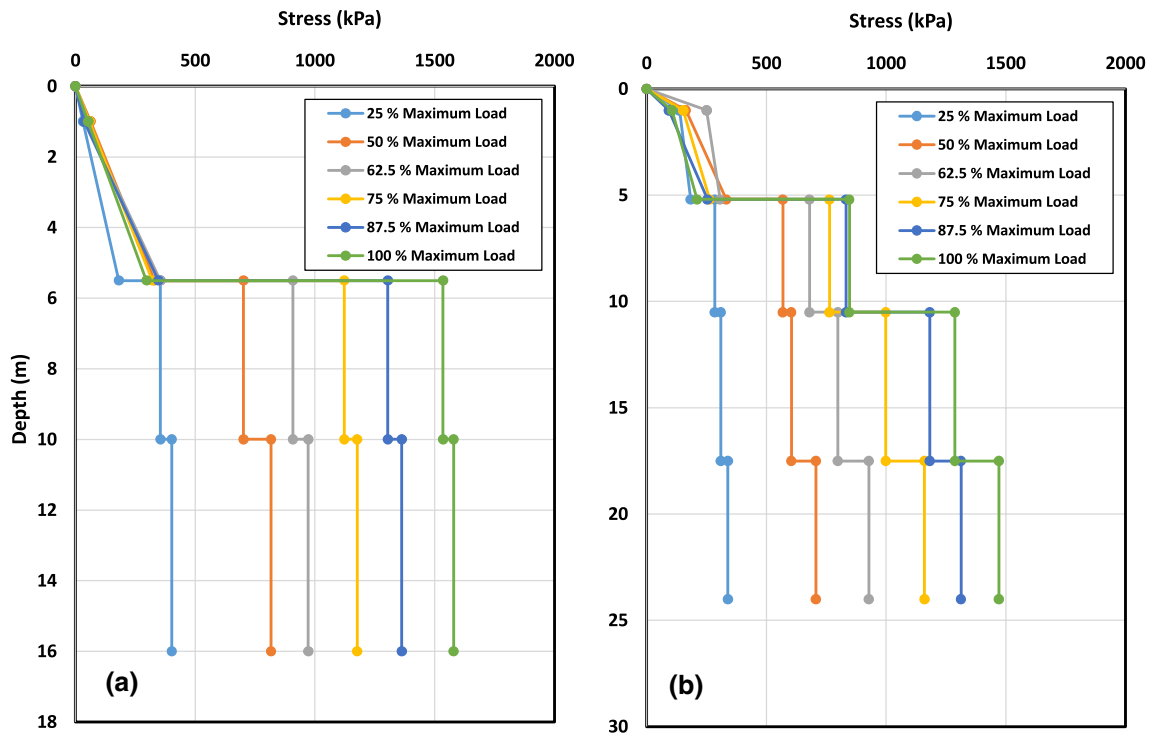


Fig. 11 a Shaft Resistance versus depth for a pile P1 and b pile P2

Table 4 Variation of stress in rock vs. depth for piles P1 and P2 at the maximum applied loads

Pile P1		Pile P2	
Depth (m)	Side Resistance (kPa)	Depth (m)	Side Resistance (kPa)
5.5–10	1535	5.2–10.5	847
10–16	1579	10.5–17.5	1288
		17.5–24	1472

$$Q_s = f_{su} \pi d L_s \tag{1}$$

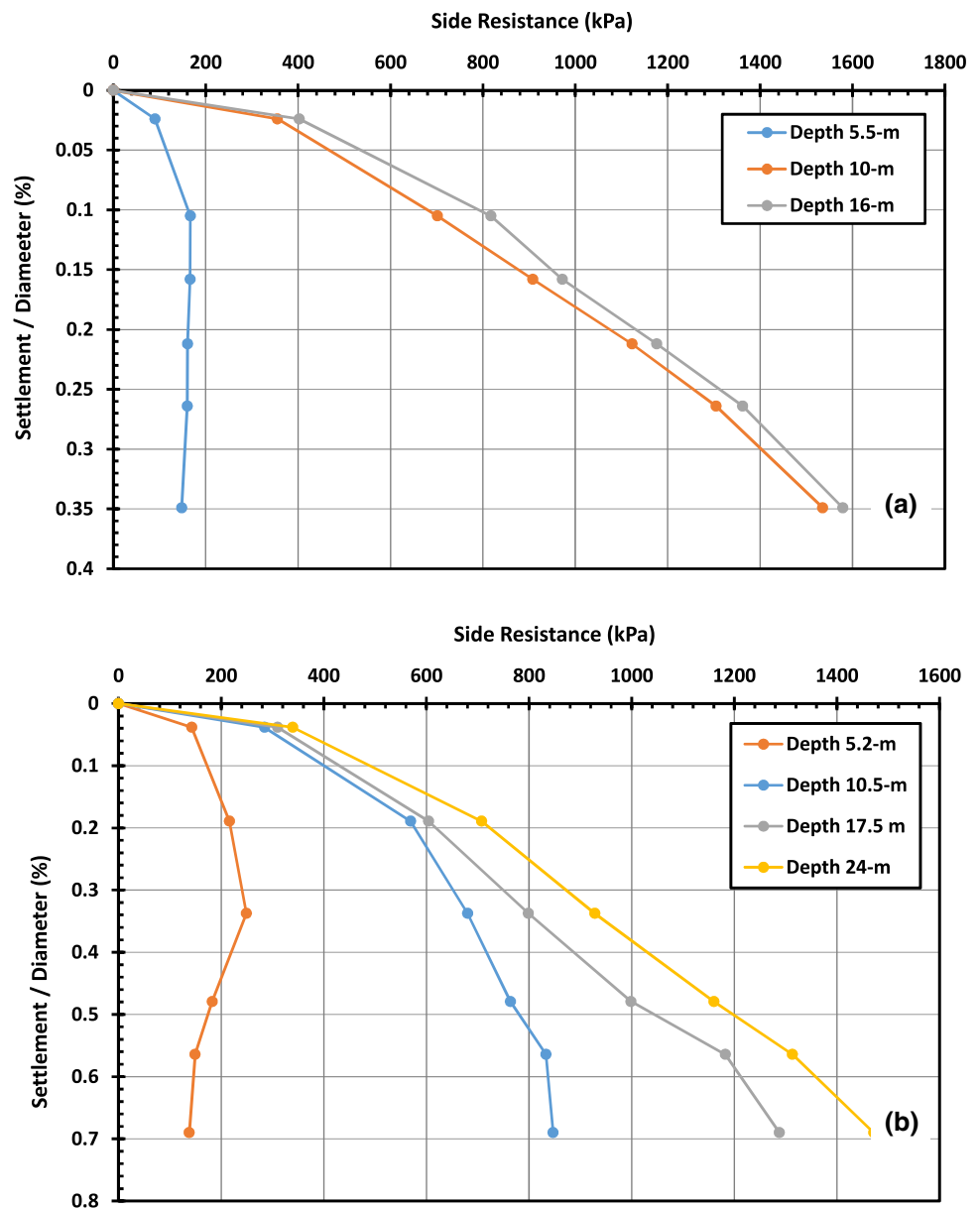
where Q_s = socket shaft resistance, f_{su} = shear side resistance along the pile–rock interface, d = pile diameter and L_s = rock socket length. Accordingly, it is important to

properly determine the shear side resistance (f_{su}) to compute the pile axial capacity. The pile side resistance is influenced by multiple factors which include rock strength, rock mass properties (e.g., RQD), shear strength between the rock and concrete interface, method of construction as it affects shaft roughness [28]. Due to the complexity of accounting for all these factors, most design methods are based on rock uniaxial strength [12, 29]. A plethora of correlations has been developed to evaluate shear side resistance in rocks [4–12, 31–33]. Table 5 summarizes some of the correlations used to calculate the pile side resistance. These correlations take the following general format:

$$f_{su} = \alpha \sigma_c^n \tag{2}$$

where σ_c is the rock unconfined compressive strength, and α and n are empirical fitting parameters. As illustrated in Table 5, the value of n ranges between 0.5 and 1. The value

Fig. 12 Shaft side resistance versus pseudo-strain for **a** pile P1 and **b** pile P2



of α varies between 0.2 and 2. These factors are based on load tests either on full scale or model piles. Some of the correlations are based on tests performed in specific rock formations or on broader databases which include results from piles socketed in different rock types. Asem [30] presents a thorough review of some of the commonly used correlations for evaluating the rock socket side resistance.

Noting the large variability in the values of α , it is important to compare their suitability for application to specific rock formations.

As illustrated earlier, none of the tested piles are loaded to failure. Thus, the ultimate side resistance is computed for each case using both Chin and Decourt methods. Figures 13-a, 13-b and 13-c shows the maximum measured stresses as

Table 5 Correlations between pile socket side resistance and rock unconfined strength

Shaft resistance	Reference
$\frac{f_{su}}{p_a} = 1.1 \left(\frac{\sigma_c}{p_a} \right)^{0.56}$ Where p_a = atmospheric pressure	Rosenberg and Journeaux [31]
$\frac{f_{su}}{p_a} = \alpha \sqrt{\frac{\sigma_c}{p_a}}$ Where p_a = atmospheric pressure and $\alpha = 0.2$ to 0.3	Horvath and Kenny [4]
$\frac{f_{su}}{p_a} = 0.45 \sqrt{\frac{\sigma_c}{p_a}}$ for regular clean socket*	Rowe and Armitage [5]
$\frac{f_{su}}{p_a} = 1.3 \sqrt{\frac{\sigma_c}{p_a}}$ Where p_a = atmospheric pressure	Fleming et al. [7]
$f_{su} = \alpha \beta \sigma_c$ Where $\alpha = f(\sigma_c)$ and $\beta = f(RQD)$	Egyptian Ministry of Housing [32]
$\frac{f_{su}}{p_a} = \sqrt{\frac{\sigma_c}{p_a}}$ Where p_a = atmospheric pressure	Kulhawy and Prakoso [8]
$\frac{f_{su}}{p_a} = 2 \sqrt{\frac{\sigma_c}{p_a}}$ Where p_a = atmospheric pressure	Fleming et al. [9]
$f_{su} = 0.3 \sigma_c$	Stark et al. [10]
$\frac{f_{su}}{p_a} = \sqrt{\frac{\sigma_c}{p_a}}$ Where p_a = atmospheric pressure	AASHTO [11]
$\frac{f_{su}}{p_a} = \sqrt{\frac{\sigma_c}{p_a}}$ Where p_a = atmospheric pressure	Brown et al. [12]
$f_{su} = e^{-1.29} \sigma_c^{0.83}$ Where f_{su} and σ_c are in MPa	Asem and Gardoni [33]

* According to Brown et al. [12], roughened socket resistance is to be considered only when artificial roughening is applied by the use of grooving tools or other techniques to increase the pile side resistance

well as Chin and Decourt resistances for the tested piles, respectively. The maximum measured resistance is 55% and 52% of Chin and Decourt ultimate loads, respectively. Both Chin and Decourt ultimate resistances are close with Decourt higher by 6% on average.

The back-calculated side resistance values are compared with those calculated using the empirical correlations as shown in Fig. 14. The ratios of the average maximum measured resistance to the different empirical methods vary between 0.27 (relative to Fleming et al. [9]) and 0.54 (relative to Kulhawy and Prakoso [8]; AASHTO [11]; Brown et al. [12]). On average, the maximum measured resistance is 0.44 of the mean resistance from the different techniques. The ratio of Chin ultimate resistance to the empirically calculated values ranges from 0.97 (relative to Kulhawy and Prakoso [8]; AASHTO [11]; Brown et al. [12]) and 0.49 (Fleming et al. [9]). The average Chin ultimate resistance is 0.79 compared to the mean of the empirically evaluated values. Similarly, the ratio of Decourt’s ultimate resistance is 1.03 relative to the resistance obtained using Kulhawy and Prakoso [8]; AASHTO [11]; and Brown et al. [12] and

0.52 relative to Fleming et al. [9]. The correlation proposed by Kulhawy and Prakoso [8] and adopted by both AASHTO [11]; Brown et al. [12] provides the closest prediction of the socket side resistance obtained using either Chin or Decourt techniques. On the other hand, Fleming et al. [9] overestimate the side resistance by approximately 100% compared to either Chin or Decourt techniques. Based on the current study, Eq. (3) is recommended for use to compute the shaft resistance of piles socketed in Dubai limestone:

$$f_{su} = \alpha \sigma_c^{0.5} \tag{3}$$

where $\alpha = 0.97$ to 1.03 with an average of 1.0 .

Summary and conclusions

The results of eight full-scale pile load tests socketed in weak rock are analyzed. Two of the piles are instrumented to model the load transfer with depth along the pile shaft. The subsurface ground is comprised of a fill layer underlain with sand which extends to an average depth of 5.5-m

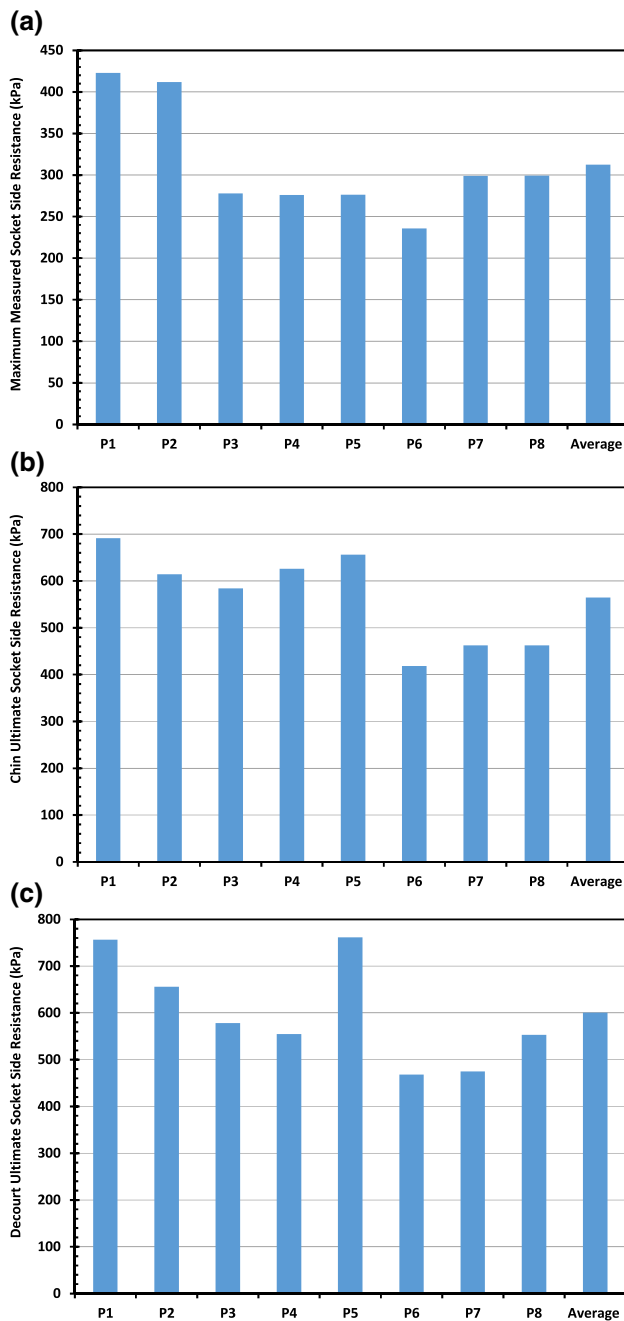
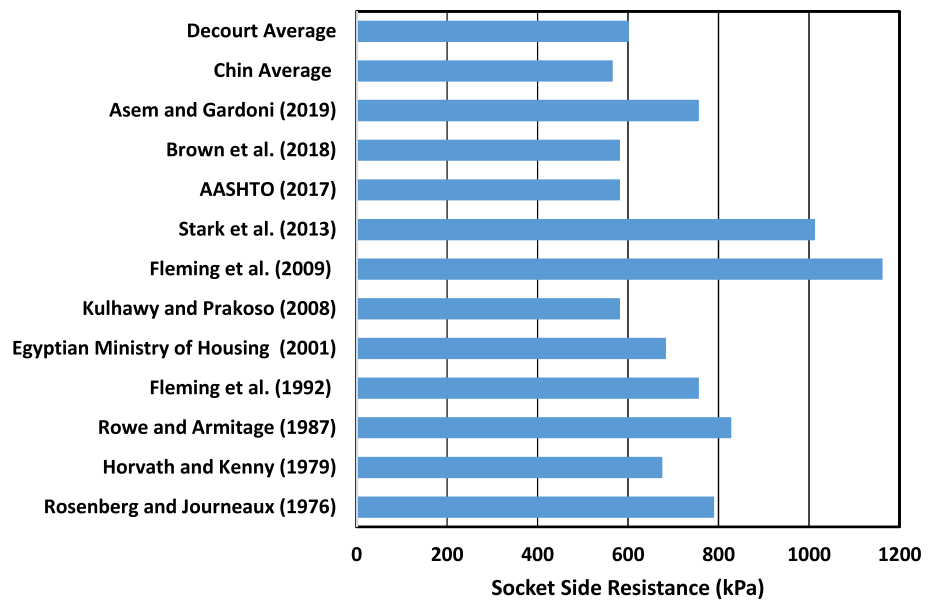


Fig. 13 **a** Maximum measured side resistance; **b** Chin ultimate side resistance; and **c** Decourt ultimate side resistance

underlain by very weak to weak limestone with an average RQD of 77%. The pile diameters are 1-m and 1.2-m with socket lengths ranging between 11.5-m and 19.8-m. Based on the analysis of the pile load test results, it is shown that none of the piles reached failure. Chin [23] and Decourt [26] techniques are used to evaluate the ultimate pile capacities providing close results. Therefore, it is concluded that either methods can be used to calculate a reasonable evaluation of capacity. Based on the instrumented pile load test data, it is shown that the pile side resistance in the upper sand layer peaks at a pseudo-strain ranging between 0.11% and 0.34%, while the ultimate side resistance in the rock layer is not reached up to the maximum recorded strains of 0.35% and 0.69%. Furthermore, the resistance within the sand layer is quite small compared to that of rock so it may be neglected. It is also noted that no load is transferred to the pile tip up to the maximum measured pile pseudo-strains which range between 0.35 and 0.69%. A comparison is made between the measured pile side resistance and those obtained from empirical correlations based on the rock unconfined compressive strength. The equation proposed by Fleming et al. [9] overestimates the pile resistance by approximately a factor of 1.9. Both Chin and Decourt ultimate resistances compare well with the method proposed by Kulhawy and Prakoso [8] and adopted by AASHTO [11] and Brown et al. [12]. A correlation between the shaft side resistance and the rock unconfined compressive strength is proposed for piles socketed in Dubai limestone.

Fig. 14 Comparison between the empirically calculated side resistances compared with the maximum measured, Chin and Decourt resistances



Declarations

Conflict of interest On behalf of the author, the corresponding author states that there is no conflict of interest.

References

- Carrubba P (1997) Skin friction of large-diameter piles socketed into rock. *Can Geotech J* 34:230–240
- Akguner C, Kirkit M (2012) Axial bearing capacity of socketed single cast-in-place piles. *Soils Found* 52(1):59–68
- Gutiérrez-Ch JG, Senent S, Melentjevic S, Jimenez R (2021) A DEM-based factor to design rock-socketed piles considering socket roughness. *Rock Mech Rock Eng* 54:3409–3421
- Horvath RG, Kenney TC (1979) Shaft resistance of rock-socketed drilled piers, In: *Proceedings of symposium on deep foundations*, ASCE, pp. 182–214
- Rowe RK, Armitage HH (1987) Theoretical solutions for axial deformation of drilled shafts in rock. *Can Geotech J* 24(1):126–142
- Reese LC, O’Neill MW (1988) *Drilled shafts: construction procedures and design methods*, Report No. FHWA-HI-88-042, FHWA, Washington, DC., p 564
- Fleming WGK, Weltman AJ, Randolph MF, Elson WK (1992) *Piling Engineering*, 2nd edn. Blackie & Son Ltd., London
- Kulhawy FH, Prakoso W (2008) Issues in evaluating capacity of socketed rock foundations, In: *The 12th international conference of international association for computer methods and advances in geomechanics (IACMAG)*, Goa, India, pp 3297–3298
- Fleming WGK, Weltman AJ, Randolph MF, Elson WK (2009) *Piling Engineering*, 3rd edn. Taylor & Francis, London
- Stark TD, Long JH, Asem P (2013) *Improvements for determining the axial capacity of drilled shafts in shale in Illinois*. Illinois Department of Transportation Report No. FHWAICT-13-017, Illinois, IL, United States
- AASHTO (2017) *AASHTO LRFD bridge design specifications 8th edition*. American Association of State Highway and Transportation Officials, 1781 p
- Brown DA, Turner JP, Castelli RJ, Loehr JE (2018) *Drilled shafts: construction procedure and design methods*. Report No. FHWA NHI-18-024, U.S. Department of Transportation Federal Highway Administration, 756 p
- Yamin M, Khan Z, El Naggar H, Al Hai N (2018) Nonlinear regression analysis for side resistance of socketed piles in rock formations of Dubai Area. *J Geotech Geol Eng* 36:3857–3869
- Poulos HG, Davids AJ (2005) *Foundation design for the Emirates Twin Towers*. Dubai Canadian Geotech J 42:716–730
- Poulos HG, Bunce G (2008) *Foundation design for the Burj Dubai – The world’s tallest building*. In: *Sixth international conference on case histories in geotechnical engineering*, Arlington, VA, August 11–16, Paper No. 147, 16 p
- Poulos HG (2018) A review of geological and geotechnical features of some middle eastern countries. *J Innov Infrastruct Solut* 3:51. <https://doi.org/10.1007/s41062-018-0158-z>
- Mayne PW, Christopher BR, DeJong J (2001) *Manual on subsurface investigations*, national highway institute, Publication No. FHWA NHI-01-031, Federal Highway Administration, Washington, DC. 305 p
- National Engineering Handbook – Part 631 – Geology* (2012). Chapter 4: engineering classification of rock materials. United States Department of Agriculture Natural Resources Conservation Service. 61 p
- Le Tirant P, Nauroy J-F (1994) *Design guides for offshore structures: foundations in carbonate soils*, Technip Editions, 204 p
- ASTM D1143 / D1143M-20, *Standard Test Methods for Deep Foundation Elements Under Static Axial Compressive Load*, ASTM International. West Conshohocken, PA, 2020, www.astm.org.
- Brinch Hansen J (1963) Discussion of hyperbolic stress-strain response: cohesive soils. *J Soil Mech Found Div* 89(4):241–242
- De Beer EE (1970) Experimental determination on the shape factors and the bearing capacity factors of sand. *Geotechnique* 2(4):387–411
- Chin FK (1971) Discussion to “Pile tests: Arkansas river project.” *ASCE J Soil Mech Found Div* 97(6):930–932
- Vesic AS (1973) Analysis of ultimate loads of shallow foundations. *J Soil Mech Found Div*, ASCE 99(1):45–73

25. Amar S, Baguelin F, Canepa Y, Frank R (1994) Experimental study of the settlement of shallow foundations. *Vert Horiz Deform Found Embankments*, ASCE, Reston 2(40):1602–1610
26. Decourt L (1999) Behavior of foundations under working load conditions. In: *Proceedings of the XI Panamerican conference on soil mechanics and geotechnical engineering*, Foz do Iguassu, Brazil, vol. 4, pp 453–487
27. Elhakim AF (2005) Evaluation of shallow foundation displacements using soil small-strain stiffness. Doctoral Dissertation, Georgia Institute of Technology, Atlanta, Georgia, USA, 406 p
28. Gannon JA, Masterton GGT, Wallace WA, Muir Wood D (1999). *Piled foundations in weak rock*, Report 181, CIRIA, 144 p
29. Turner J (2006). *Rock-socketed shafts for highway structure foundations*. *Transp Res Board*, 137 p
30. Asem P (2018). *Axial behavior of drilled shafts in soft rock*. PhD dissertation. University of Illinois at Urbana-Champaign, USA, 3603 p
31. Rosenberg P, Journeaux NL (1976) Friction and end bearing tests on bedrock for high capacity socket design. *Can Geotech J* 13(3):324–333
32. Egyptian Ministry of Housing (2001) Egyptian code of practice for soil mechanics and foundations. *Deep Foundations*, part 4/202. The Arab Republic of Egypt, Housing & Building National Research Center.
33. Asem P, Gardoni P (2019) Evaluation of peak side resistance for rock socketed shafts in weak sedimentary rock from an extensive database of published field load tests: a limit state approach. *Can Geotech J* 56(12):1816–1831